AJNR Am J Neuroradiol 23:1187–1198, August 2002

Detection and Characterization of Very Small Cerebral Aneurysms by Using 2D and 3D Helical CT Angiography

J. Pablo Villablanca, Reza Jahan, Parizad Hooshi, Silvester Lim, Gary Duckwiler, Aman Patel, James Sayre, Neil Martin, John Frazee, John Bentson, and Fernando Viñuela

BACKGROUND AND PURPOSE: **Many cases of subarachnoid hemorrhage are due to rupture of small cerebral aneurysms. Our purpose was to evaluate the usefulness of helical CT angiography (CTA) in the detection and characterization of very small (<5 mm) intracranial aneurysms.**

METHODS: **One hundred eighty consecutive patients underwent CTA for suspected intracranial aneurysms. All aneurysms prospectively detected by CTA were confirmed by digital subtraction angiography (DSA) or at surgery. CT angiograms and digital subtraction angiograms were reviewed by two independent blinded radiologists who performed aneurysm detection, quantitation, and characterization using 2D multiplanar reformatted and 3D volume-rendering techniques.**

RESULTS: **Fifty-one patients harboring 41 very small intracranial aneurysms were included in this series. Eighty-one percent (33 of 41 aneurysms) were ≤4 mm in maximal diameter, and 37% (15 of 41 aneurysms) were ≤3 mm in maximal diameter. Sensitivity of CTA for very small intracranial aneurysm detection ranged from 98% to 100% (95% confidence intervals, 0.871, 0.999, 0.914, and 1.0), compared with 95% for DSA. The specificity of CTA and DSA for very small intracranial aneurysms was 100% (26 of 26 aneurysms). Positive predictive value ranged from 98% to 100%. Negative predictive value ranged from 96% to 100%. Accuracy of CTA for detection of very small intracranial aneurysms was 99% and 100% ($\kappa = 0.969 - 1.0 \pm 0.1221$). Forty-eight percent of aneurysms were detected in the presence of subarachnoid hemorrhage.**

CONCLUSION: **The sensitivity of CTA for the detection of cerebral aneurysms ≤5 mm is higher than that of DSA, with equal specificity and high interoperator reliability. High quality, noninvasive CTA aneurysm detection and characterization can be performed using routine clinical CT scanners and commercially available image processing workstations.**

Subarachnoid hemorrhage (SAH) related to ruptured aneurysm kills >10,000 North Americans each year (1). Conventional angiography, generally selective intra-arterial digital subtraction angiography (DSA), has been the criterion standard for the detection and characterization of intracranial aneurysms (1). The primary advantage of DSA over other imaging modalities is the high resolution achieved by most systems, generally providing 0.3-mm resolution by using a 1024 × 1024 matrix. This high resolution translates into relatively high sensitivity and specificity for aneurysm detection, with a reported 5% to 10% false negative rate (2). The false negative rate is generally due not to limitations of spatial resolution but to physical limitations of the angiographic equipment that may make it difficult to obtain the optimal projection needed to detect some intracranial aneurysms (3, 4). In other cases, it is not possible to know a priori which is the specific projection that will render an aneurysm visible, again leading to false negative findings (4, 5). Furthermore, once an aneurysm is detected, accurate visualization and measurement of the aneurysm neck and its relationship to the parent artery may be difficult or impossible to obtain in ≤11% of cases (3), impairing selection of the optimal treatment method (5).

DSA has several additional disadvantages, including the high skill level that is required to perform the

Received August 9, 2000; accepted after revision January 7, 2002.

From the Departments of Radiological Sciences (J.P.V., R.J., P.H., S.L., G.D., A.P., J.S., F.V., J.B.) and Neurosurgery (N.M., J.F.), University of California, Los Angeles, Los Angeles, CA.

Address reprint requests to J. Pablo Villablanca, MD, Department of Radiological Sciences, University of California, Los Angeles, 10833 Le Conte Avenue, Box 951721, Los Angeles, CA 90095.

procedure, invasiveness requiring arterial puncture and intra-arterial catheter manipulation, and comparatively high procedural cost. Arterial puncture and catheter manipulation are associated with a low but significant 1% complication risk and a 0.5% rate of permanent neurologic deficit (6).

Helical CT angiography (CTA) is a comparatively new noninvasive volumetric imaging technique. Images can be safely obtained by a trained technologist without the need for arterial puncture or catheter manipulation. CTA is not associated with significant patient risks (7). Furthermore, CTA image acquisition requires an imaging time of ≤1 minute (8–10).

Once acquired, CTA data can be viewed from unlimited projections in both 2D and 3D modes, facilitating the task of aneurysm detection (11, 12). In some centers, CTA has been reported to be the only study performed before surgery in a significant number of cases (12) and has been shown to reveal aneurysms when DSA results are negative (13). Others question the usefulness of CTA in the detection of very small aneurysms (VSA), generally defined in the literature as measuring <5 mm, citing a comparative lack of published studies focusing on this size group (8). Using four readers and a sample size of 47 aneurysms, Kogori et al (14) recently reported a mean sensitivity of 64% for very small intracranial aneurysms and 100% for large aneurysms, with disappointing 17% false negative and 15% false positive rates. In a study of 40 patients reported by Anderson et al (11), only four of seven cerebral aneurysms ≤3 mm in diameter detected by DSA were found using CTA. Similar results were obtained by Schwartz et al (15). Other investigators using older protocols have found high false negative rates for skull base lesions near bone (16, 17).

If a technique is to serve as a noninvasive replacement for DSA in the detection and characterization of intracranial aneurysms, the sensitivity and specificity of that technique for very small intracranial aneurysms should ideally be equal to or higher than those of DSA. Our purpose was to evaluate the usefulness of CTA for patients with very small intracranial aneurysms by using optimized acquisition and postprocessing protocols.

Methods

Study Design

Between June 1997 and May 2000, a total of 180 consecutive patients underwent CTA for suspected or known intracranial aneurysms. Criteria for inclusion in the study required both CTA and conventional DSA studies. If the DSA was found to be negative and the CTA positive, the patients also had to undergo surgery (coiling or clipping) for inclusion in the study. Patients were selected by the referring physicians for CTA on the basis of clinical history, including symptoms and signs suggestive of aneurysm, such as headache or cranial neuropathy, presentation to the emergency department with SAH confirmed by unenhanced CT or lumbar puncture, or a previous routine CT scan or MR image suggesting the presence of an intracranial aneurysm. Informed consent was obtained for all diagnostic angiography. Data were gathered and analyzed with approval of the Institutional Human Subjects Protection Committee.

All CT angiograms were interpreted prospectively in a blinded manner by a neuroradiologist. All cases with confirmed CTA study results were also reviewed retrospectively by a second independent blinded neuroradiologist. The second reader interpreted the CT angiograms in random order. Both readers had no knowledge of the clinical history or of the results of any previous imaging studies. DSA studies were prospectively and independently interpreted in a blinded manner by a single expert.

An aneurysm was defined as a saccular outpouching from a parent artery, having a clearly definable sac and neck. Infundibula were excluded from the study and were defined as a pyramidal dilatation at the origin of a vessel with an artery arising from the apex. Aneurysmal dilatations, defined as abnormal outpouching of an artery wall but without a definable neck, were not considered aneurysms (18). An aneurysm was considered fully characterized if all three orthogonal dimensions could be obtained, the aneurysm neck could be well visualized and measured, mural calcification and intraluminal thrombi could be detected and their distribution relative to the aneurysm neck described, and arterial incorporations into the aneurysm sac or neck could be detected and mapped precisely (10). Aneurysm characterization was confirmed by DSA or by direct intraoperative visualization or both.

Helical CT Angiography Protocol

All CTA studies were performed using a helical technique with routine clinical GE Hi-Speed or GE CTI single detector scanners (General Electric, Milwaukee, WI). All patients were positioned supine, with head immobilization achieved using adhesive tape. A timing run was performed for all patients, using a 10-second upfront delay, 15 dynamic images, total volume injected of 15 cc, injection rate of 3 cc/s, 80 kV, and 80 mA. The helical technique included a pitch of 1.0 to 1.5, 1-mm section collimation, 0.5-mm reconstruction interval, coverage from the bottom of the anterior arch of C1 to the midlateral ventricles (average acquisition time, 60 seconds), a matrix of 512 × 512, a 180-mm field of view, 120 kV, and 260 to 290 mA. The infusion of 350 mg I/mL solution (Nycomed Inc., Princeton, NJ) of contrast material was IV injected through a 22-gauge antecubital angiocatheter by using a power injector at a rate of 3 cc/s. Image reconstruction was accomplished by using a soft-tissue kernel and 180-degree linear interpolation.

Image Processing

Image postprocessing was performed using a Food and Drug Administration approved, commercially available, Vitrea workstation, versions 1.1 and 1.2 (Vital Images, Minneapolis, MN), operating on a Silicon Graphics O2 board (Silicon Graphics, Mountainview, CA). Three-dimensional perspective volume-rendered images (window [W] = 250, level [L] = 150), 3D thick slab and gray scale 2D single section images, and thick slab multiplanar reformatted 2D images (W = 1000, L = 500) were evaluated. Single section 2D and thick slab 3D multiplanar reformatted images were used for aneurysm detection, for quantitation of the aneurysm sac, to obtain aneurysm neck and parent artery dimensions, and to determine the presence, location, and extent of mural calcification and intraluminal thrombi with respect to the aneurysm neck. Curved oblique multiplanar reformatted images along with 2D single section multiplanar reformatted data were used to detect and characterize extradural-intraosseous aneurysms. Volume-rendered 3D images were used for intradural aneurysm detection, characterization of arterial branching patterns at the neck, 3D visualization of mural thrombi and calcification, depiction of the position and spatial orientation of the aneurysm neck and sac, and depiction of the relationship of the aneurysm to local and regional bone anatomy. The arterial trees were examined

to fourth order bifurcations in the anterior circulation and to third order branching in the posterior circulation. All CTA quantitation was made using the internal digital caliper, with linear accuracy of ±10% for measures <2 mm and ±4% for measurements between 2 and 10 mm. The time required for the complete systematic examination and documentation of each case by each blinded reader was recorded and mean analysis times calculated.

Digital Subtraction Angiography

DSA consisted of three- or four-vessel, multiple projection, biplane angiography performed by neuroradiologists using the Seldinger technique, and femoral percutaneous catheterization. Oblique and ×2 to ×3 magnification views were routinely obtained to clarify aneurysm anatomy. All DSA quantitation was performed by an interventional neuroradiologist gathering measurements in standard orthogonal projections by using the pixel count method or the reference method described by Fernandez-Zubillaga et al (3).

Statistical Analysis

Data were analyzed using standard contingency tables. One- and two-sided 95% (exact) confidence intervals were calculated for each independent reader for each statistical parameter. The κ statistic and its SD were used to determine interoperator agreement. Very small intracranial aneurysms discovered by CTA had to be confirmed by DSA or at surgery to be included in the study. Patients with negative CTA and DSA results defined the control population (true negatives). Patients with positive CTA and DSA results or surgically proven intracranial aneurysms served as true positives. CTA false negatives were defined as negative CTA results in cases with aneurysms found at surgery or by using DSA. CTA false positives were defined as positive CTA results in cases in which DSA or surgery were negative for aneurysms. DSA false negatives were defined as negative DSA results in cases with surgically proven aneurysms.

Results

CTA prospectively detected 54 very small intracranial aneurysms in 34 of 180 patients (28 female and six male patients). Four patients each with single aneurysms underwent MR angiography only for lesion confirmation (declined DSA) and were therefore excluded from the study. Three patients had basilar tip aneurysms that were detected by CTA but not by DSA. Two of these patients each had dual incidental aneurysms but did not undergo confirmatory surgery and were therefore excluded. The third patient had multiple aneurysms, all except one of which was detected by both CTA and DSA. Therefore, this incidental aneurysm not found by DSA and not operated on was also excluded from the study. Three patients harboring a total of four aneurysms underwent CTA and then directly received surgical treatment (declined DSA) and were also excluded. Therefore, nine of 34 patients harboring a total of 13 aneurysms were excluded from the initial study group.

The remaining 25 patients harboring 41 aneurysms underwent both CTA and DSA or DSA and surgery (when DSA results were negative) and are the basis for this study. The average patient age for the very small intracranial aneurysm population (20 female and five male patients) was 54 years (age range, 32–83 years). Twenty-four percent of the patients in this consecutive series were known by the enrolling physicians but not by the blinded readers to have aneurysms, based on previous CT or MR imaging studies.

Thirty-four of the 180 patients had negative CTA results. Eight patients with negative CTA results declined DSA. Therefore, 26 of 34 patients with negative CTA results underwent DSA and served as negative controls for this study (16 female and 10 male patients). The average patient age for the control population was 57 years (age range, 14–85 years).

Systematic examination and documentation of the data sets required 6 to 36 minutes (average, 16 minutes) of image processing by the neuroradiologist. No further pre- or postprocessing of the images was performed by the readers or any other personnel.

Table 1 lists the aneurysms by location, sac size, neck size, and dome-to-neck ratio. The average maximal aneurysm sac diameter was 3.48 mm (range, 1.7–5.0 mm). The average aneurysm neck size was 3.03 mm (range, 1.7–5.0 mm). Eighty-one percent (33 of 41 aneurysms) were ≤4 mm in maximal diameter, and 37% (13 of 41 aneurysms) were ≤3 mm in maximal diameter. Ten percent of the aneurysms (four of 41 aneurysms) were ≤2 mm. Seventy-one percent (29 of 41 aneurysms) were supraclinoid (intradural), and 29% (12 of 41 aneurysms) were infraclinoid (extradural). The most common location was the middle cerebral artery (MCA) bifurcation at 24% (13 of 54 aneurysms) (Table 2). Single very small intracranial aneurysms were seen in 68% (17 of 25 patients), whereas 32% harbored multiple very small intracranial aneurysms (eight of 25 patients). The smallest aneurysm was located in the right supraclinoid internal carotid artery and measured 1.9 × 1.6 × 1.3 mm, with a neck measuring 1.7 mm (Fig 1).

Thirty-nine aneurysms were confirmed by DSA. Two aneurysms found by CTA were not revealed by DSA (in patients 8 and 14). These two patients were treated surgically on the basis of CTA information alone and were confirmed to have the aneurysms that had been identified by CTA. Patient 8 had negative results of a single DSA study that was performed 2 days before CTA, and patient 14 had negative results of DSA studies that were performed 2 and 5 days before CTA. Patient 8 had a 4.9-mm anteriorly projecting anterior communicating artery aneurysm, and patient 14 had a laterally projecting 2.7-mm MCA bifurcation aneurysm. In this case, CTA clearly showed a 3.5-mm anterior communicating aneurysm and the smaller left MCA bifurcation aneurysm. The CTA study did not clearly depict a 1-mm placoid aneurysmal dilatation adjacent to the true aneurysm (Fig 2). Both DSA negative cases presented with SAH, and both were treated by neurosurgical clipping.

One aneurysm was not identified on CT angiograms by reader 1 (aneurysm 32, patient 18). This was a 2.7-mm right MCA bifurcation aneurysm in a patient with a large ipsilateral arteriovenous malformation. Subsequent analysis of the data set revealed that the aneurysm was clearly present on the 2D and 3D

TABLE 1: Characteristics of patients who underwent CTA

Aneurysm (no.)	Patient (no.)	Age (y)/Sex	Clinical History	Aneurysm Location	CTA Result	Sac Size AP × TR × CC (mm)	Aneurysm Characterization Neck Size (mm)	Dome/ Neck	C/T/AI	DSA Result	Therapy
1	1	39/M	AVM	R C-O	+	2.5 × 2.5 × 2.5	2.5	1.0	−/−/−	+	Follow-up
2	2	48/F	Multiple a.	Acom	+	3.1 × 4.2 × 2.3	4.3	1.0	−/−/+	+	Follow-up
3	3	45/M	SAH	L Acho	+	3.4 × 2.6 × 3.3	2.2	1.5	−/−/−	+	Coil
4	3			L A2	+	2.8 × 2.0 × 2.9	3.0	1.0	−/−/−	+	Coil
5	3			R A1	+	3.3 × 2.6 × 4.2	2.4	1.8	−/−/−	+	Follow-up
6	3			L M1	+	3.2 × 3.9 × 4.0	4.1	1.0	−/−/−	+	Follow-up
7	4	62/F	TIA	L C-O	+	2.4 × 2.5 × 2.6	2.6	1.0	−/−/−	+	Follow-up
8	5	58/F	Amaurosis	Bas tip	+	3.4 × 2.9 × 4.0	2.4	1.7	−/−/−	+	Follow-up
9	6	32/M	SAH	L MCB	+	3.0 × 3.0 × 4.0	3.0	1.3	−/−/−	+	Coil
10	7	58/F	H/A	R C-O	+	2.8 × 3.3 × 2.5	3.2	1.0	−/−/+	+	Follow-up
11	7			R ICAB	+	3.8 × 3.1 × 3.2	2.6	1.5	−/−/−	+	Follow-up
12	7			L C-O	+	2.3 × 3.1 × 2.4	4.1	0.8	−/−/−	+	Follow-up
13	7			Basilar a.	+	3.5 × 3.2 × 3.9	3.3	1.2	−/−/−	+	Coil
14	8	47/F	SAH	Acom	+	4.9 × 2.8 × 2.8	4.9	1.0	−/−/−	−	Clip
15	9	54/F	AVM	R S Hyp	+	3.5 × 3.1 × 1.7	2.5	1.4	−/−/−	+	Follow-up
16	9			L S Hyp	+	3.5 × 4.2 × 2.1	3.0	1.4	−/−/−	+	Follow-up
17	10	42/F	Multiple a.	L MCB	+	3.8 × 3.2 × 2.3	3.3	1.2	−/−/−	+	Clip
18	11	71/F	CNP	L SICA	+	3.0 × 2.8 × 2.9	2.6	1.2	−/−/−	+	Follow-up
19	12	51/F	Blindness	R Acho	+	3.3 × 3.5 × 4.4	3.1	1.4	−/−/−	+	Clip
20	12			R C-O	+	3.1 × 3.0 × 3.1	2.0	1.6	−/−/−	+	Clip
21	12			R SICA	+	1.9 × 1.6 × 1.3	1.7	1.1	−/−/−	+	Clip
22	12			R Pcom	+	3.3 × 2.9 × 3.2	3.0	1.1	−/−/−	+	Clip
23	12			Acom	+	4.7 × 3.4 × 3.6	2.4	2.0	−/−/−	+	Clip
24	13	56/F	AVF	R S Hyp	+	2.7 × 3.6 × 2.0	2.5	1.4	−/−/−	+	Follow-up
25	14	63/F	SAH	R MCB	+	2.2 × 2.4 × 2.7	2.4	1.1	−/−/−	−	Clip
26	15	51/F	SAH	R C-O	+	2.1 × 1.7 × 2.5	2.7	0.9	−/−/−	+	Follow-up
27	15			R C-O	+	2.0 × 1.8 × 1.0	2.0	1.0	−/−/−	+	Follow-up
28	16	35/F	SAH	R SICA	+	2.6 × 2.6 × 3.5	3.5	1.0	−/−/−	+	Clip
29	17	40/F	SAH	R MCB	+	2.8 × 2.7 × 3.1	3.1	1.0	−/−/−	+	Follow-up
30	17			R MCB	+	2.5 × 4.7 × 2.9	3.4	1.4	−/−/−	+	Follow-up
31	18	68/M	SAH	ACom	+	3.0 × 2.8 × 3.5	2.4	1.5	−/−/−	+	Follow-up
32	18			R MCB	−	2.2 × 2.7 × 2.3	2.3	1.2	−/−/+	+	Follow-up
33	19	28/F	H/A	L C-O	+	2.7 × 2.1 × 1.9	1.8	1.5	−/−/−	+	Follow-up
34	20	47/F	SAH	R SICA	+	2.7 × 2.4 × 2.9	3.9	0.7	−/−/−	+	Clip
35	21	62/M	Multiple a.	R MCB	+	4.4 × 3.2 × 4.1	4.6	1.0	−/−/−	+	Follow-up
36	21			R Pcom	+	3.4 × 3.0 × 3.4	3.5	1.0	−/−/−	+	Follow-up
37	21			L Pcom	+	3.0 × 2.5 × 3.2	3.7	0.9	−/−/−	+	Follow-up
38	22	83/F	SAH	R CICA	−	3.9 × 2.0 × 3.3	3.5	1.1	−/−/−	+	Follow-up
39	23	63/F	SAH	R MCB	+	2.2 × 3.8 × 3.6	3.6	1.1	−/−/−	+	Clip
40	24	79/F	SAH	R SICA	+	2.0 × 1.6 × 1.6	2.0	1.0	−/−/−	+	Follow-up
41	25	74/F	Multiple a.	L MCB	+	1.5 × 1.9 × 0.9	1.7	1.0	−/−/−	+	Follow-up

Note.—CTA indicates CT angiography; DSA, digital subtraction angiography; AP, anteroposterior; TR, transverse; CC, craniocaudad; C, calcification; AI, arterial incorporation; AVM, arteriovenous malformation; C-O, caroticoophthalmic artery; multiple a, multiple aneurysms; Acom, anterior communicating artery; SAH, subarachnoid hemorrhage; L, left; Acho, anterior choroidal artery; A2, second segment of the anterior cerebral artery; R, right; A1, first segment of the anterior cerebral artery; M1, first segment of the middle cerebral artery; TIA, transient ischemic attack; Bas tip, basilar tip; MCB, middle cerebral artery bifurcation; H/A, headache; ICAB, internal carotid artery bifurcation; Basilar a, basilar artery; S Hyp, superior hypophyseal artery; CNP, cranial nerve palsy; SICA, supraclinoid internal carotid artery; Pcom, posterior communicating artery; CICA, cavernous internal carotid artery.

CT angiograms but was overlooked during the initial reading (Fig 3). Reader 2 detected this lesion as well as all other aneurysms present. The sensitivity, specificity, positive predictive value, negative predictive value, and accuracy of CTA versus DSA and surgery are shown in Tables 3 (reader 1) and 4 (reader 2). There were no CTA or DSA false positive results. Similar values for DSA versus CTA and surgery are shown in Table 5.

The total number of aneurysms receiving invasive therapy was 37% (15 of 41 aneurysms). Four aneurysms were treated by coil embolization (10%). Of these, three presented with SAH. Twenty-seven percent (11 of 41 aneurysms) were clipped neurosurgically, and 36% of these presented with SAH. Figure 4 (patient 6) shows a representative example of very small intracranial aneurysm detection by CTA in the setting of severe SAH and vasospasm, with DSA correlation.

Overall, 37% (19 of 51 patients) of all patients in the series presented with SAH. Twenty-seven percent (seven of 26 patients) of patients with confirmed

TABLE 2: Location of aneurysms <5 mm maximal diameter (n = 41)

Location	Frequency
Middle cerebral artery bifurcation	9 (22%)
Caroticoophthalmic	8 (21%)
Anterior communicating artery	5 (12%)
Supraclinoid internal carotid artery	5 (12%)
Superior hypophyseal artery	4 (10%)
Posterior communicating artery	3 (8%)
Internal carotid artery bifurcation	1 (2.5%)
Anterior choroidal artery	1 (2.5%)
M1 segment of middle cerebral artery	1 (2.5%)
Cavernous internal carotid artery	1 (2.5%)
A1 segment of the anterior cerebral artery	1 (2.5%)
A2 segment of the anterior cerebral artery	1 (2.5%)
Basilar artery	1 (2.5%)

negative CTA results and 48% (12 of 25 patients) of patients harboring very small intracranial aneurysms presented with SAH. A total of 44% (18 of 41 aneurysms) of all very small intracranial aneurysms were detected by CTA in the presence of subarachnoid blood. The incidence of SAH that was thought to be due to very small intracranial aneurysm rupture among the study population was 14% (seven of 51 patients). Of the 19 patients presenting with SAH, 37% of the cases were thought to be due to a very small intracranial aneurysm rupture and 63% of the cases were thought to be due to the rupture of another aneurysm >5 mm in maximal diameter. The overall incidence of SAH due to very small intracranial aneurysms in the larger aneurysm population was 4.8% (seven of 146 patients). Three of these seven patients harbored multiple intracranial aneurysms but did not otherwise share demographic features.

In 76% of the aneurysm cases, CTA and the confirmatory study were performed within 5 days. In the remaining cases, CTA and the confirmatory study were separated by >5 days. There were no complications related to CTA or DSA studies. There were no CTA or DSA technical failures. Interpretation of CTA images was provided immediately for all urgent cases and within 96 hours after study completion when the patient was not stable for treatment or was not otherwise immediately scheduled for treatment.

Pairwise interobserver agreement between independent CTA readers was 0.969 ± .1221, indicating excellent reliability. The 95% confidence interval for each statistical parameter was also excellent for both CTA and DSA (Tables 3, 4, and 5)

Table 1 provides additional information regarding the ability of CTA to characterize VSAs, including the presence or absence of arterial segments incorporated into the aneurysm sac or neck, mural thrombi, calcification at the aneurysm sac, and dome-to-neck ratios. Arterial incorporations occurred in only 7% of the cases (three of 41 cases). Neither mural thrombi nor calcification occurred in any case of VSA. The high correlation between CTA and DSA studies is exemplified in Figure 5. The ability of CTA to characterize intracavernous aneurysms is illustrated in Figure 6.

To establish the necessity of performing a timing run before performing CTA, we analyzed the relationship between individual patient timing injection delays and patient age and gender. The injection delay times for a random sample of 150 CTA cases were collected and tabulated versus patient age and sex and by frequency (Fig 7). The analyses showed a wide variation of total delay times, with a 90% confidence interval between 11 and 33 seconds. A statistically significant ($P < .001$) but slight ($P = .31$) correlation was observed between patient age and total injection delay, with age explaining only 10% of the variation in the delay times.

Discussion

A detection rate for VSA equal to or better than DSA is essential if CTA is to serve as a noninvasive replacement for DSA. This study showed that the current technology for 2D and 3D helical CT image acquisition and postprocessing is capable of providing that sensitivity when expert readers conduct both CTA and DSA interpretation. A detection rate equal to DSA for even very small cerebral aneurysms ensures a central role for CTA in the evaluation of all patients with symptomatic, and potentially asymptomatic, intracranial aneurysms. Our results showed that the technique is also able to accurately describe all aspects of an aneurysm, including branching pat-

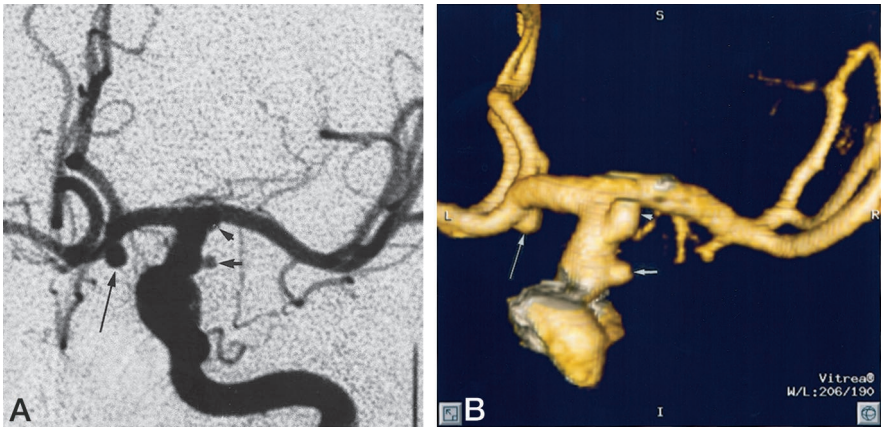

FIG 1. Patient 12, aneurysm 21. Example of smallest aneurysm seen in this study.

A, Midarterial phase anteroposterior projection DSA image shows a small saccular aneurysm at the supraclinoid internal carotid artery (*short arrow*). Note larger anterior communicating artery aneurysm (*long arrow*). Anterior choroidal artery aneurysm is mostly obscured by overlying internal carotid artery bifurcation (*arrowhead*).

B, 3D posteroanterior projection CTA image with lateral angulation shows aneurysm sac (*short arrow*). Anterior communicating artery (*long arrow*) and anterior choroidal artery (*arrowhead*) aneurysms are also well seen.

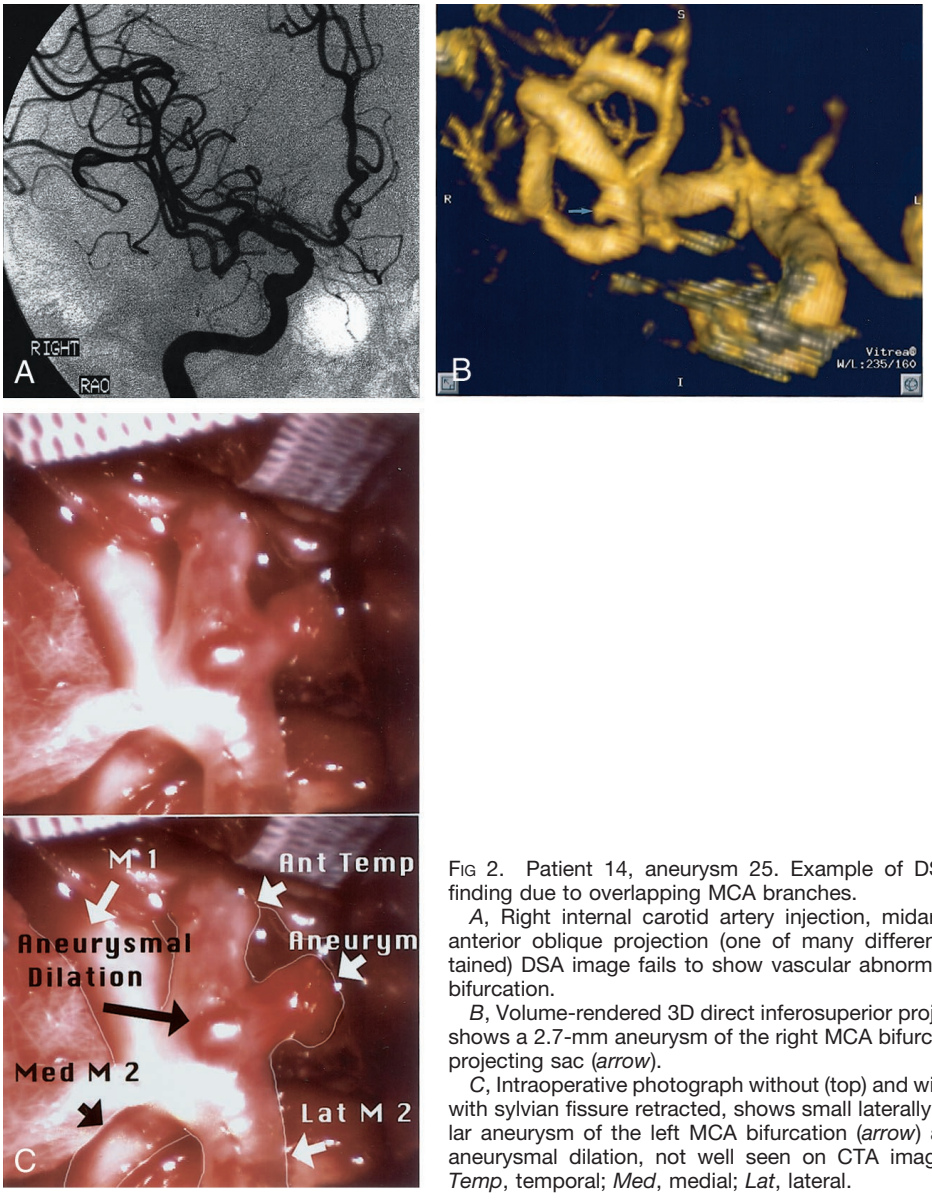

FIG 2. Patient 14, aneurysm 25. Example of DSA false negative finding due to overlapping MCA branches.

A, Right internal carotid artery injection, midarterial phase right anterior oblique projection (one of many different projections obtained) DSA image fails to show vascular abnormality at right MCA bifurcation.

B, Volume-rendered 3D direct inferosuperior projection CTA image shows a 2.7-mm aneurysm of the right MCA bifurcation with laterally projecting sac (*arrow*).

C, Intraoperative photograph without (top) and with (bottom) labels, with sylvian fissure retracted, shows small laterally projecting saccular aneurysm of the left MCA bifurcation (*arrow*) and small placoid aneurysmal dilation, not well seen on CTA images. *Ant*, anterior; *Temp*, temporal; *Med*, medial; *Lat*, lateral.

tern at the neck and presence of arterial incorporations into the aneurysm sac, and to determine the presence of mural calcium and thrombi. This study and previous work (9, 10, 19, 20) showed that CTA is capable of accurate aneurysm characterization.

Once gathered, CTA images can be used to triage the patient between endovascular and neurosurgical options after clinical consultation with endovascular therapists and neurosurgeons. CTA can also serve as a high quality treatment planning tool once the treatment option has been selected (10, 19).

To our knowledge, this comparative analysis of CTA and DSA in the evaluation of VSAs is the largest published. The population is also significant because 13 aneurysms were <3 mm in *maximal* diameter, a dimension threshold for which more favorable reports on CTA visualization are needed (11) and for which few reports of successful characterization are found (13, 18).

The higher sensitivity and specificity reported herein are the direct result of technical evolutions in image acquisition and postprocessing algorithms that have become available since the earliest reports (17). Others have shown that studies using newer image acquisition and analysis protocols can yield impressive results (12), indicating that protocol optimization is leading to progressively higher quality CTA. For single detector helical studies, we suggest a section collimation of ≤ 1 mm, a 0.5-mm reconstruction interval, a pitch of ≤ 1.5, an mA of ≥ 280, a matrix size of $\geq 512 \times 512$, and a field of view just large enough to include superficial temporal arteries, in case this vessel is required for an intracranial-extracranial bypass procedure (generally 18 cm). These scanning parameters allow a high spatial resolution with no appreciable z axis blurring and function for both standard single detector and newer multi-detector helical scanners. All single section helical scanners are currently able to perform to these specifications or better.

Analysis of the methods of previous investigators

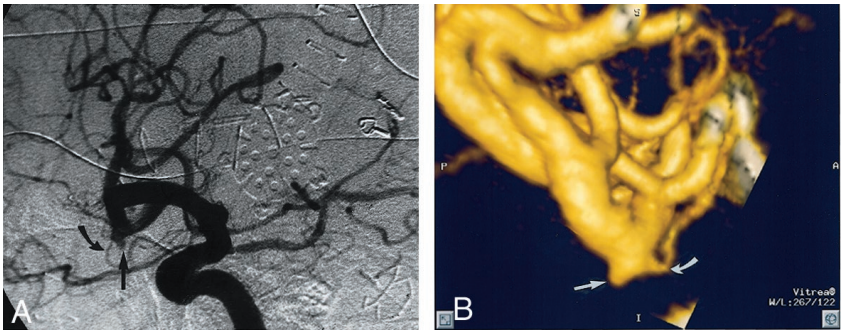

FIG 3. Patient 18, aneurysm 32. Example of CTA false negative (reader 1) finding.

A, Midarterial phase right anterior oblique projection DSA image shows a small pyramidal aneurysm sac projecting inferiorly from the anterior M2 division (*straight arrow*). Note the small anterior temporal branch arising from the neck region (*curved arrow*).

B, 3D lateromedial projection CTA image clearly shows the pyramidal aneurysm sac (*straight arrow*), along with a 0.5-mm anterior temporal branch arising from the region of the aneurysm neck (*curved arrow*). The aneurysm is clearly present but was overlooked during the initial reading by reader 1.

TABLE 3: Findings at CTA vs those at DSA and Surgery (reader 1)

	DSA and Surgery		
CTA	Aneurysm not present	Aneurysm present	Total
Aneurysm not present	26	1	27
Aneurysm present	0	40	40
Total	26	41	67

Note.—95% confidence interval (* one-sided 97.5% CI), sensitivity = 40/41 = 0.98 (.871, 0.999), specificity = 26/26 = 1.0 (.868, 1.0), positive predictive value = 40/40 = 1.0 (.912, 1.0), negative predictive value = 26/27 = 0.96 (.810, 0.999), accuracy = 26 + 40/67 = 0.99 (.919, 0.999), kappa ± SD = 0.969 ± .1221.

TABLE 4: Findings at CTA versus those at DSA and those surgery (reader 2)

	DSA and Surgery		
CTA	Aneurysm not present	Aneurysm present	Total
Aneurysm not present	26	0	26
Aneurysm present	0	41	41
Total	26	41	67

Note.—97.5% confidence interval (all one-sided), sensitivity = 41/41 = 1.0 (.914, 1.0), specificity = 26/26 = 1.0 (.868, 1.0), positive predictive value = 41/41 = 1.0 (.914, 1.0), negative predictive value = 26/26 = 1.0 (.868, 1.0), accuracy = 67/67 = 1.0 (.946, 1.0), kappa ± SD = 1.0 ± .1221.

TABLE 5: Findings at DSA vs those at CTA and surgery

	CTA and Surgery		
DSA	Aneurysm not present	Aneurysm present	Total
Aneurysm not present	26	2	28
Aneurysm present	0	39	39
Total	26	41	67

Note.—95% confidence interval (* = 97.5% one-sided), sensitivity = 39/41 = 0.95 (.835, 0.994), specificity = 26/26 = 1.0 (.868, 1.0), positive predictive value = 39/39 = 1.0 (.9.0, 1.0), negative predictive value = 26/28 = 0.93 (.765, .001), accuracy = 65/67 = 0.97 (.896, .996), kappa ± SD = .938 ± .1219.

with poor detection rates for small aneurysms reveals suboptimal scan parameters. Kogori et al (14) used a comparatively low mA and a low contrast material injection rate. Both factors may have led to their lower reported sensitivities for VSAs. In addition, in the performance of blinded screening studies, the imaging slab should be ≥90 mm, the average distance required to cover from the extradural vertebral arteries (bottom of anterior arch of C1 on lateral CT scout) to the third and fourth order sylvian branches. This span has previously been shown to include 99% of all berry aneurysm sites (21). The importance of adequate slab size is emphasized by the results of Kogori et al (14), who did not detect posterior fossa aneurysms because the inferior border of the imaging slab began above the level of the posteroinferior cerebellar artery origins. Anderson et al (11) used a small scan volume, a large field of view, and a small total contrast bolus when reporting a low sensitivity for small aneurysms. These factors directly negatively impacted the amount of intracranial circulation examined and both spatial and contrast resolution, respectively.

Another important protocol variable is the delay time selected before initiating the helical scan. Previous investigators have used empirical fixed injection delays ranging between 15 and 45 seconds (15, 20). We concur with those who indicate that a timing run or automatic peak opacification-sensing software should always be used (11). This is to ensure dynamic scanning during peak intraluminal contrast attenuation, minimal radiation exposure, and minimal total contrast material dose. In a random sample of 150 timing injection delays, we found a widely distributed range of injection delays. Clinically derived patient injection delays correlated poorly with age and gender (Fig 6, *1–3*), emphasizing the importance of avoiding use of empirical injection delay values, which may result in decreased sensitivity (12). Furthermore, the injection rate should be ≥3 cc/s (11) to achieve reasonably homogeneous vascular opacification.

In this study, accurate diagnoses were made in 21 patients in the setting of SAH, including in 14 patients harboring 21 VSAs and seven patients without intracranial aneurysms, indicating that intracranial blood does not impact the sensitivity or specificity of CTA. This is supported by other published reports (8, 14, 15). We think this is because the CT attenuation of cisternal blood is lower than that of the enhanced vessels in all cases, and this difference can be easily

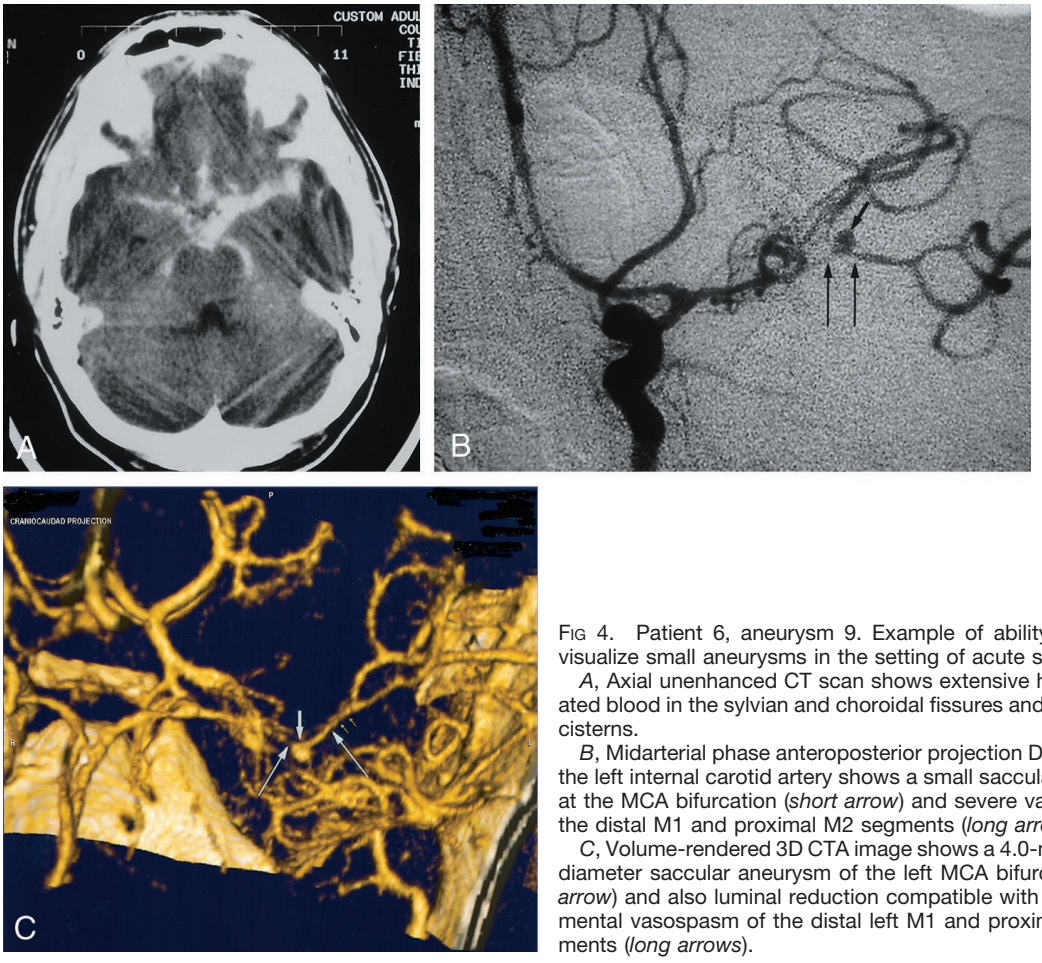

FIG 4. Patient 6, aneurysm 9. Example of ability of CTA to visualize small aneurysms in the setting of acute severe SAH.

A, Axial unenhanced CT scan shows extensive hyperattenuated blood in the sylvian and choroidal fissures and in the basal cisterns.

B, Midarterial phase anteroposterior projection DSA image of the left internal carotid artery shows a small saccular aneurysm at the MCA bifurcation (*short arrow*) and severe vasospasm of the distal M1 and proximal M2 segments (*long arrows*).

C, Volume-rendered 3D CTA image shows a 4.0-mm maximal diameter saccular aneurysm of the left MCA bifurcation (*short arrow*) and also luminal reduction compatible with severe segmental vasospasm of the distal left M1 and proximal M2 segments (*long arrows*).

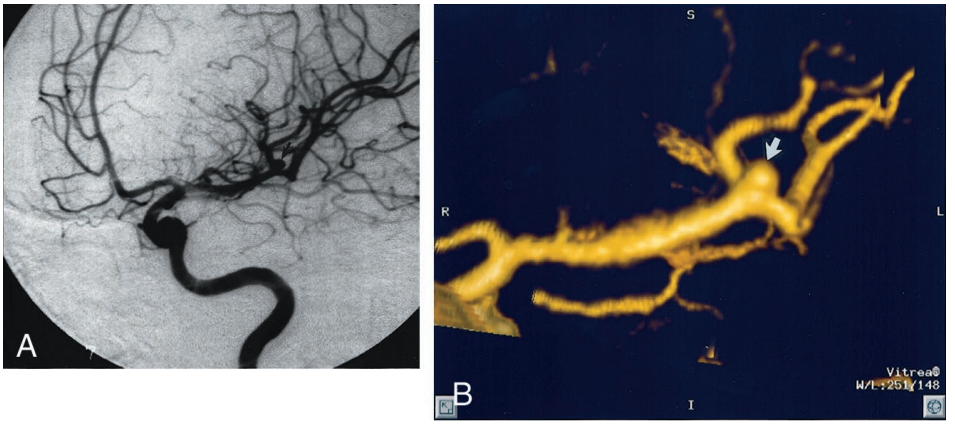

FIG 5. Patient 25, aneurysm 41. Example of high correlation between DSA and 3D CTA.

A, Midarterial phase anteroposterior oblique projection DSA image of the left MCA shows a small MCA bifurcation aneurysm (*arrow*).

B, 3D CTA image, obtained in a projection similar to that of the DSA image shown in *A*, shows a 1.9-mm maximal diameter saccular aneurysm arising from the left MCA bifurcation (*arrow*).

appreciated when the appropriate window and level settings are selected (Fig 4).

Our results also indicate that the sensitivity and characterization ability of CTA is equally high for both intradural and extradural aneurysms. Approximately 44% (17 of 41 aneurysms) were near or surrounded bone, yet all were detected. This group included carotico-ophthalmic, superior hypophyseal, cavernous carotid, carotid cave, and posterior communicating artery aneurysms. Previous authors have experienced false negative results when aneurysm is near bone (14, 15, 22). These authors seem to have used surface-shaded display techniques or volume-rendering techniques alone for aneurysm detection. Our postprocessing technique includes a systematic review of all extradural locations for possible skull base lesions using the gray scale 2D multiplanar reformatted images and is similar to that used by other authors reporting high sensitivity for aneurysms at the carotid siphon (23). Close examination of the 2D images is crucial to decreasing interpretive errors (24). We used standardized window and level settings (approximate W = 1000 and L = 500) for viewing all gray scale 2D image data. Using comparable settings,

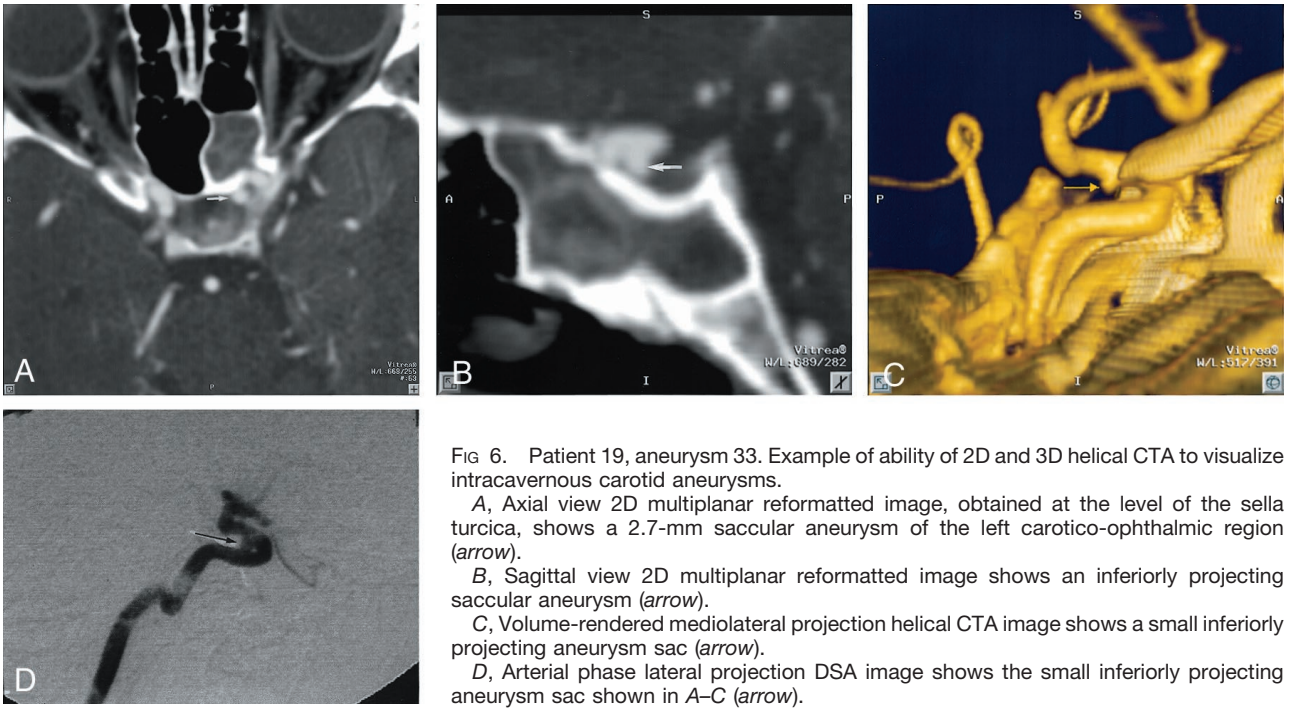

FIG 6. Patient 19, aneurysm 33. Example of ability of 2D and 3D helical CTA to visualize intracavernous carotid aneurysms.

A, Axial view 2D multiplanar reformatted image, obtained at the level of the sella turcica, shows a 2.7-mm saccular aneurysm of the left carotico-ophthalmic region (*arrow*).

B, Sagittal view 2D multiplanar reformatted image shows an inferiorly projecting saccular aneurysm (*arrow*).

C, Volume-rendered mediolateral projection helical CTA image shows a small inferiorly projecting aneurysm sac (*arrow*).

D, Arterial phase lateral projection DSA image shows the small inferiorly projecting aneurysm sac shown in *A–C* (*arrow*).

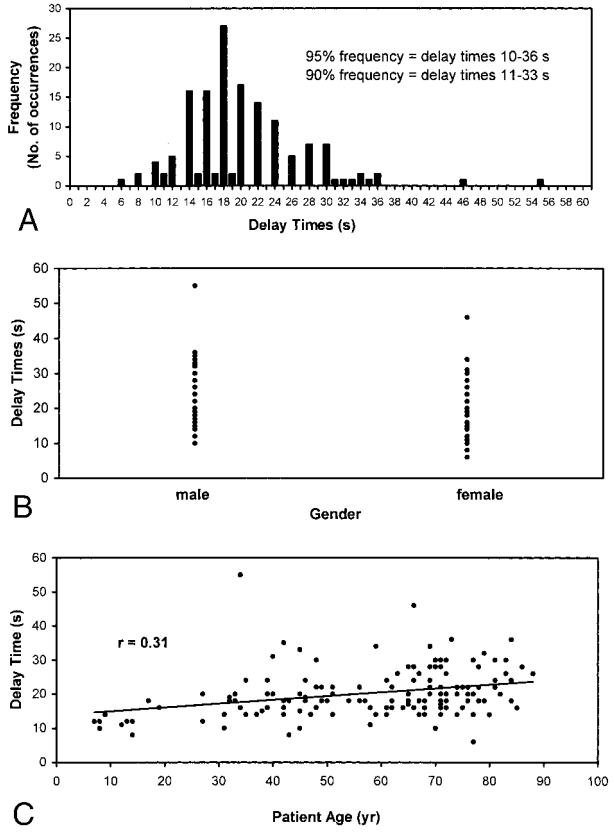

FIG 7. Characterization of injection delay times.

one can clearly differentiate the density of bone (1800–4000 HU) from that of contrast opacified blood (150–450 HU). The use of intracavernous fatty tissue, which separates cavernous venous sinusoids from intracavernous carotid aneurysms, can greatly facilitate aneurysm detection in this region (Fig 6). The cross-referencing tool, used to confirm or exclude the presence of a suspected lesion by visual confirmation of an abnormality in all three major planes, is also essential for aneurysm detection in this location. In general, we did not find the volume-rendered 3D images to be useful in this location, because it decreased lesion conspicuity by artifactually fusing vascular and bone anatomy.

In this study, the sensitivity for VSA detection was higher with CTA than with DSA. This difference reflects the limitations of DSA when the ideal projection necessary to visualize the aneurysm sac cannot be obtained or is not routinely obtained as part of an aneurysm workup. For these small lesions, this may occur when there is superimposition of normal vessels over the region of interest (3, 4) or when an ideal projection cannot be obtained because of the rotational limits of the C-arm fluoroscope or complex local arterial anatomy (8, 13).

Vascular superimposition occurred in both cases that had false negative DSA results. For patient 14, a patient with a right MCA bifurcation aneurysm, the complex branching pattern at the bifurcation obscured the lesion on multiple magnified projections (Fig 2). The optimal view by CTA was directly inferior, with some lateral angulation, a difficult projection to obtain by catheter angiography. The lesion was proven at surgery. The other lesion was at the anterior communicating artery, where lesions may be obscured by overlapping vessels or by inadequate opacity at the anterior communicating artery when a cross-compression view is required but not obtained or is suboptimal. Other locations where small aneurysms can be missed by DSA include the basilar tip when the sac projects directly anteriorly or posteriorly and only straight anteroposterior and lateral views are

obtained and the posterior communicating artery when there is poor filling of that vessel in the setting of balanced flow. The single instance of a false negative CTA result was a case of oversight on the part of reader 1; the lesion is clearly visible on the 3D volume-rendered images (Fig 3). This suggests that with adequate attention and scrutiny, all clinically relevant aneurysms can be detected by CTA using routine scanners, the protocols outlined herein, and commercially available image processing workstations. In this case, the aneurysm was overlooked on initial review because reader 1 became distracted by a large anterior circulation arteriovenous malformation and the ensuing search for intranidal aneurysms.

The arrival of CTA as a viable noninvasive imaging alternative to DSA is timely when one considers the difficulties in selecting the optimal treatment strategy for incidental cerebral aneurysms. These difficulties are in part due to a lack of knowledge regarding their natural history (25). Previous studies suggest that incidental aneurysms rupture at rates of ≥3% per year (26). The critical size at which aneurysms are at a significant risk of rupture has been reported to be 4 mm (27). More recently, the International Study of Unruptured Intracranial Aneurysm Investigators (28), using a large sample size, concluded that the cumulative rate of rupture of aneurysms <10 mm in diameter at diagnosis is <0.05% per year for those with no history of aneurysmal subarachniod hemorrhage and 0.5% per year for those with history of aneurysmal SAH. In our study, the frequency of SAH attributable to VSA was significant and suggests that size alone may not provide a complete basis on which to evaluate the individual risk of aneurysm rupture.

Previous work has shown that CTA can be used for both diagnosis and treatment planning in the acute setting (10). If conservative treatment is selected, CTA can also serve as the noninvasive follow-up study of choice. CTA can be safely acquired by a trained technologist, does not require arterial puncture, is not associated with significant patient risks, and correlates highly with DSA images (Fig 5). In a prospective study of 4875 patients, the incidence rates of acute and late adverse reactions to IV administered low osmolal nonionic contrast agent were 1.2% and 4.7%, respectively, with most reactions being minor (nausea, mild vomiting, urticaria), 0.2% of reactions being intermediate (edema of face or glottis, bronchospasm, severe vomiting), and no major complications (cardiac arrest, arrhythmias, pulmonary edema, collapse) (7). Furthermore, CTA requires a scan time of ≤1 minute (8–10). The radiation dose from high resolution neuro-CTA has been shown to be more than that of conventional CT but less than that of DSA (29). We use a low kVp, low mA technique for determining patient-specific timing to minimize radiation exposure. Although we have not experienced any significant adverse events with our CTA protocol, care must be exercised for patients with advanced renal insufficiency, congestive heart failure, and contrast material allergies. We advise angling the x-ray beam away from radiation-sensitive tissues, such as the cornea and lens, for patients returning for sequential follow-up studies.

With DSA, aneurysm sac and neck dimensions may be difficult to measure directly because there is generally no internal image scale. A formula for measurement of aneurysm necks with DSA has been proposed that uses assumed diameters for known major intracranial arterial segments (3). These diameters are derived primarily from published histopathologic studies. The accuracy of this method can be compromised by any condition that alters reference vessel diameter, including atherosclerotic arterial stenosis or ectasia, vasospasm, gender differences, and arteriovenous malformations. Using autopsy specimens, Black et al (30) showed that the neck of most aneurysms more resembles an irregular ellipsoid than a circle. Therefore, different DSA angiographic projections will provide different diameters. These problems do not occur with CTA data sets, which are digital and can be measured and reformatted in any plane. CTA orthogonal or oblique cross-sectional views accurately reveal both the diameter and the 2D contour of any aneurysm neck.

Table 1 shows that CTA is able to provide both full aneurysm quantitation, including dome-to-neck ratios, and full aneurysm characterization, including the presence or absence of mural thrombi and calcium, and the possibility of incorporated arterial segments. This information can then be used by both neurosurgeons and endovascular therapists for decision making regarding the optimal treatment modality (10). Recently, Velthuis et al (12) reported that 45% of 51 patients were successfully surgically treated on the basis of CTA information alone.

Previous investigators have shown that aneurysms with dome-to-neck ratios >2 show high rates of permanent occlusion with endovascular coiling techniques (3). Table 1 shows that four patients, all with dome-to-neck ratios <2, were treated by endovascular coiling, indicating that other factors, such as poor neurologic status and co-morbid conditions, may also have affected the selection of the treatment option. The incidence of arterial incorporations was low in this VSA population, and no cases were found exhibiting mural calcification or thrombi, indicating that these variables may be expected to play a lesser factor in selecting a treatment option when the lesion is a VSA. This is in contrast to larger aneurysms, which have been shown to display mural calcification or intraluminal thrombi in ≤15% of cases (10).

Regarding postprocessing, every effort should be made to obtain the best available postprocessing workstation. The workstation should be fast and capable of performing high quality perspective 3D volume rendering and orthogonal and curved oblique 2D multiplanar image reformatting. In addition, the device must have an internal digital caliper and the ability to cross reference between orthogonal multiple reformatted views for rapid confirmation of suspected lesions in multiple projections. Rather than a fixed number of standard viewing projections, as some investigators have used (14), we prefer a systematic but

free-form examination of the image data in both 2D and 3D. This can be performed rapidly in cine mode. Our image analysis times ranged from 6 to 36 minutes, with an average of 16 minutes. The longer analysis times were for patients with up to six intracranial aneurysms each.

We have used only perspective volume rendering to view 3D data because this technique makes available all the voxels within a volume, avoiding extensive loss of information, potentially arbitrary vessel border definition, vessel-bone interface difficulties, and loss of perspective, which are inherent to shaded surface display and maximum intensity pixel techniques (31, 32). Volume rendering is now the preferred rendering technique for CTA (33). The 3D images were most useful for detecting and characterizing intradural lesions that are obvious when viewed in a 3D environment but inconspicuous when viewed in a 2D mode. In this series, an aneurysm was discovered only by using the 3D images in 10% of the cases, with subsequent lesion confirmation and quantitation using 2D sections. This is because of the high spatial complexity of the 2D vascular image data in some locations, particularly the MCA bifurcations, anterior communicating artery, basilar tip, and foramen magnum regions. This is supported by reports of similarly diminished detection rates, also in the range of 90%, when only the CTA source images are examined (34). The most important role of 3D is to facilitate a thorough understanding of the shape of the aneurysm sac and neck and of the spatial relationship of the sac to the surrounding branches and local bone anatomy.

In contrast to the methods used by other authors who use consensus reading of CTA data (14), we selected an independent blinded image review method. This approach may more closely parallel the image interpretation patterns observed in daily radiology practice, in which a single clinician must rely on his or her abilities and knowledge to reach a diagnosis, thus allowing a more rigorous evaluation of the merits and limitations of helical CTA. In addition, we did not use confidence intervals in our evaluations because we think that method provides little clinical realism. Either an aneurysm can be clearly seen on the 2D multiplanar and 3D data sets or it cannot, and DSA must therefore be performed. The high confidence of the readers of the CTA data is shown by the ability to fully characterize each aneurysm, including aneurysm neck size, branch incorporations, and presence or absence of mural calcification and thrombi, and by the high concordance between the readers.

The high sensitivity and high specificity of aneurysm detection for neuroradiologists emphasizes the user-friendliness of the technique and the relatively high conspicuity of even these very small lesions when using optimized image acquisition and analysis protocols. Nevertheless, CTA, like DSA, is a spatially complex dataset that requires expert readers for optimal interpretation.

Our study design had several limitations. First, the study was prospective but not randomized, because the ordering physicians selected the patients for study, possibly introducing a selection bias for patients most likely to benefit from CTA study. This limitation is tempered by the wide range of aneurysmal pathology represented in the study sample and by the fact that only 24% of the lesions were previously known to the ordering physician. The study is also limited by a possible sampling error, because not all patients studied by CTA agreed to undergo DSA. This limitation could affect our sensitivity and specificity, if the cases excluded from the study population differed substantially from those included in the final study group. A DSA sensitivity that is in general agreement with those of previous reports serves to mitigate this weakness, because it suggests that the general performance of DSA was accurately represented by our study population.

In conclusion, this study shows that the sensitivity of CTA for the detection of VSA is higher than that of DSA and that the specificity of CTA for VSA is equal to that of DSA and significantly higher than previously reported. We also show that CTA is able to provide complete aneurysm characterization and that image acquisition and processing can be performed rapidly on commercially available devices. CTA image information has been shown to determine the choice of treatment and to assist in treatment planning.

References

1. King JT Jr. **Epidemiology of aneurysmal subarachnoid hemorrhage.** *Neuroimaging Clin N Am* 1997;7:659–668
2. Tatter SB, Crowell RM, Ogilvy CS. **Aneurysmal and microaneurysmal "angio-negative" subarachnoid hemorrhage.** *Neurosurgery* 1995;37:48–55
3. Fernadez Zubillaga A, Guglielmi G, Viñuela F, Duckwiler GR. **Endovascular occlusion of intracranial aneurysms with electrically detachable coils: correlation of aneurysm neck size and treatment results.** *AJNR Am J Neuroradiol* 1994;15:815–820
4. Zouaoui A, Sahel M, Marro B, et al. **Three-dimensional computed tomographic angiography in detection of cerebral aneurysms in acute subarachnoid hemorrhage.** *Neurosurgery* 1997;41:125–130
5. Debrun GM, Aletich VA, Kehrli P, Misra M, Ausman JI, Charbel F. **Selection of cerebral aneurysms for treatment using Guglielmi detachable coils: the preliminary University of Illinois at Chicago experience.** *Neurosurgery* 1998;43:1281–1295
6. Heiserman JE, Dean BL, Hodak JA, et al. **Neurologic complications of cerebral angiography.** *AJNR Am J Neuroradiol* 1999;15:1401–1411
7. Mikkonen R, Kontkanen T, Kivisaari L. **Acute and late adverse reactions to low-osmolal contrast media.** *Acta Radiol* 1995;36:72–76
8. Lenhart M, Bretschneider T, Gmeinwieser J, et al. **Cerebral CT angiography in the diagnosis of acute subarachnoid hemorrhage.** *Acta Radiol* 1997;38:791–796
9. Velthuis BK, Rinkel GJ, Ramos LP, et al. **Subarachnoid hemorrhage: aneurysm detection and preoperative evaluation with CT angiography.** *Radiology* 1998;208:423–430
10. Villablanca JP, Martin N, Jahan R, et al. **Volume-rendered helical computerized tomography in the detection and characterization of intracranial aneurysms.** *J Neurosurg* 2000;93:254–264
11. Anderson GB, Findlay JM, Steinke DE, et al. **Experience with computed tomographic angiography for the detection intracranial aneurysms in the setting of acute subarachnoid hemorrhage.** *Neurosurgery* 1997;41:522–528
12. Velthuis BK, van Leeuwen MS, Witkamp TD, Ramos LM, Van Der Sprenkel JW, Rinkel GJ. **Computerized tomography angiography in patients with subarachnoid hemorrhage: from aneurysm detection to treatment without conventional angiography.** *J Neurosurg* 1999;91:761–767

13. Hashimoto H, Iida J, Hironaka Y, Okada M, Sakaki T. **Use of spiral computed tomographic angiography in patients with subarachnoid hemorrhage in whom subtraction angiography did not reveal cerebral aneurysms.** *J Neurosurg* 2000;92:278–283
14. Kogori Y, Takahashi M, Katada K, et al. **Intracranial aneurysms: detection with three-dimensional CT angiography with volume rendering: comparison with conventional angiographic and surgical findings.** *Radiology* 1999;211:497–506
15. Schwartz RB, Tice HM, Hooten SM, Hsu L, Stieg PE. **Evaluation of cerebral aneurysms with helical CT: correlation with conventional angiography and MR angiography.** *Radiology* 1994;192:717–722
16. Ogawa T, Okudera T, Noguchi K, et al. **Cerebral aneurysms: evaluation with three-dimensional CT angiography.** *AJNR Am J Neuroradiol* 1996;17: 447–454
17. Hope JK, Wilson JL, Thomson FJ. **Three-dimensional CT angiography in the detection and characterization of intracranial berry aneurysms.** *AJNR Am J Neuroradiol* 1995;17:439–445
18. Kubota T, Niwa J, Tanigawara T, Chiba M, Akiyama Y, Inamura S. **Differential diagnosis between aneurysm and infundibular dilatation in the IC-PC region with 3D CTA.** *No Shinkei Geka* 2000;28: 31–39
19. Harrison MJ, Johnson BA, Gardner GM, Welling BG. **Preliminary results on the management of unruptured intracranial aneurysms with magnetic resonance angiography and computed tomographic angiography.** *Neurosurgery* 1997;40:947–955
20. Kato T, Sano H, Katada K, et al. **Applications of three-dimensional CT angiography (3D-CTA) to cerebral aneurysms.** *Surg Neurol* 1999;52:113–121
21. Yasargil MG. *Microneurosurgery.* vol 1. New York: Georg Thieme Verlag; 1984:299
22. Imakita S, Onishi Y, Hashimoto T, et al. **Subtraction CT angiography with controlled-orbit helical scanning for detection of intracranial aneurysms.** *AJNR Am J Neuroradiol* 1998;19:291–295
23. Ochi T, Shimizu K, Yasuhara Y, Shigesawa T, Mochizuki T, Ikezoe J. **Curved planar reformatted CT angiography: usefulness for the evaluation of aneurysms at the carotid siphon.** *AJNR Am J Neuroradiol* 1999;20:1025–1030
24. Young N, Dorsch NW, Kingston RJ. **Pitfalls in the use of spiral CT for identification of intracranial aneurysms.** *Neuroradiology* 1999; 41:93–99
25. Sekhar LN, Heros RC. **Origin, growth, and rupture of saccular aneurysms: a review.** *Neurosurgery* 1981;8:248–260
26. Jane JA, Winn HR, Richardson AE. **The natural history of intracranial aneurysms: rebleeding rates during the acute and long term period and implications for surgical management.** *Clin Neurosurg* 1977;24:176–184
27. Cromptom M. **Mechanisms of growth and rupture in cerebral berry aneurysms.** *Br Med J* 1996;1:1138–1142
28. International Study of Unruptured Intracranial Aneurysms Investigators. **Unruptured intracranial aneurysms: risk of rupture and risks of surgical intervention.** *New Engl J Med* 1998;339:1725–1733
29. Shrier DA, Tanaka H, Numaguchi Y, Konno S, Patel U, Shibata D. **CT angiography in the evaluation of acute stroke.** *AJNR Am J Neuroradiol* 1997;18:1011–1020
30. Black SP, Leo H-L, Carson WL. **Recording and measuring the interior features of intracranial aneurysms removed at autopsy: method and initial findings.** *Neurosurgery* 1988;22:40–43
31. Kuszyk BS, Heath DG, Ney DR, et al. **CT angiography with volume rendering: imaging findings.** *AJR Am J Roentgenol* 1995;165:445–448
32. Johnson PT, Heath DG, Kuszyk BS, Fishman EK. **CT angiography with volume rendering: advantages and applications in splanchnic vascular imaging.** *Radiology* 1996;200:564–568
33. Kuszyk BS, Heath DG, Johnson PT, Fishman EK. **CT angiography with volume rendering: in vitro optimization and evaluation of accuracy in quantifying stenoses.** *AJR Am J Roentgenol* 1999;173: 449–457
34. Schmid UD, Steiger HJ, Huber P. **Accuracy of high-resolution computed tomography in direct diagnosis of cerebral aneurysms.** *Neuroradiology* 1987;29:152–159